INTERNATIONAL JOURNAL OF PRECISION ENGINEERING AND MANUFACTURING Vol. 19, No. 11, pp. 1699-1708 NOVEMBER 2018 / 1699

REGULAR PAPER

DOI: 10.1007/s12541-018-0197-6
ISSN 2234-7593 (Print) / 2005-4602 (Online)

A Model Prediction Control Design for Inverse Multiplicative Structure Based Feedforward Hysteresis Compensation of a Piezo Nanopositioning Stage

Min Ming[1], Jie Ling[1], Zhao Feng[1], and Xiaohui Xiao[1,2,#]

1 School of Power and Mechanical Engineering, Wuhan University, No. 8, South Donghu Road, Wuchang District, Wuhan, 430072, China
2 Shenzhen Institute of Wuhan University, China
Corresponding Author / E-mail: xhxiao@whu.edu.cn, TEL: +86-13720360269
ORCID: 0000-0002-8212-2452

KEYWORDS: Piezo-actuated stage, Hysteresis, Prandtl-Ishlinskii (P-I) model, Inverse multiplicative structure, Model predictive control

The inherent hysteresis nonlinearity of piezoelectric actuators seriously deteriorates the tracking performance of piezo-actuated nanopositioning stage, especially in large stroke applications. Usually, the model of piezo-actuated stage is given by cascading a rate-independent hysteresis submodel with a linear dynamics submodel. This paper develops a composite model predictive control (MPC) with feedforward hysteresis compensation based on the inverse multiplicative structure. The feedforward controller has the merit of non-inverse requirement. The linear MPC is utilized as a feedback controller with the feature of simple solution for the feedforward compensation system. Experimental tracking results of sinusoidal signals at different frequencies as well as complex signals show that the proposed method can improve the tracking performance of the piezo-actuated stage, verifying its effectiveness.

Manuscript received: March 31, 2018 / Revised: July 30, 2018 / Accepted: September 12, 2018

NOMENCLATURE

PID = Proportional-Integral-Derivative
SMC = Sliding Mode Control
MPC = Model Prediction Control
RMS = Root-Mean-Square

1. Introduction

Many precision instruments, such as nanomanipulators,[1,2] scanning probe microscopies (SPMs),[3] atomic force microscopes (AFMs),[4] are indispensable in various fields of engineering and science. The piezo-actuated nanopositioning stages are the core components of precision instruments. They are usually designed as flexure-hinge-guided mechanisms driven by piezoelectric actuators (PEAs) with the merits of small size, high positioning resolution and quick frequency response.[5] However, the PEAs are incapable in some high-precision situations without effective controller because of the inherent hysteresis nonlinearity.

To improve the tracking performance, a wide variety of control techniques have been developed to remove hysteresis effect in recent literatures.[6] Proportional-integral-derivative (PID) control with simple structure and straightforward implementation is widely applied in industrial applications.[7] The PID has also been used to compensate the nonlinearity of PEAs in commercial piezo-actuated stages. Due to the intrinsic defect of traditional PID, the tracking performance is limited on the low rate signals and simple trajectories. An adaptive PID[8] and a nonlinear PID with extended state observer[9] have also been adopted for better performance. To overcome such limitations, researchers have made great efforts to design control laws with some modern control techniques such as repetitive control,[10] iterative learning control,[11,12] H_∞ control,[13] and sliding mode control.[14-18] A repetitive controller (RC) is designed for tracking periodic reference trajectories for systems that exhibit hysteresis.[10] The hysteresis has effect on the stability of the designed RC. But when the hysteresis effect exceeds the maximum bound, an inverse-hysteresis feedforward controller based on the Prandtl-Ishlinskii (P-I) hysteresis model is used to compensate the nonlinearity. Feedback PID combined with iterative learning control (ILC) is adopted to compensate nonlinearity, which guarantees improvement of

performance in both single-axis tracking and biaxial contouring tasks.[11] Owing to its ease of design and robustness in the presence of disturbances, sliding mode control (SMC) has been widely used for piezo-actuated stages.[16] By considering the hysteresis as disturbance, SMC can be completed without inverse-based feedforward hysteresis compensator. The effect of conventional SMC compromises with its two disadvantages, namely the infinite settling time and the chattering phenomenon.[19] Many researchers aim to obtain a finite-time convergent, chattering-free robust control by overcoming the two shortcomings. For example, a high-order adaptive terminal SMC is presented for single-input single-output uncertain nonlinear systems.[20] This approach combines the high-order SMC for finite convergence time and terminal SMC for chattering phenomenon.

Recently, model predictive control (MPC) has been successfully applied to compensate hysteresis nonlinearity of PEAs.[21] Moreover, MPC has a well-established theoretical foundation and has demonstrated great performance in the industrial applications owing to its robustness and disturbance rejection properties.[22-24] A MPC is applied in digital sliding mode control to reduce the error bound and to attenuate the chattering effect.[25] It is combined with a digital integral terminal sliding mode control to further mitigate the control error as well.[26] Besides, the MPC can deal with physical constraints in the generation of control actions or signals. An inverse-based MPC is presented, [27] in which it is used to deal with a linear dynamics submodel. Hysteresis compensation is realized through inverse feedforward of the ferromagnetic hysteresis model. A nonlinear MPC method is realized through solving a complicated nonlinear optimization problem.[28] In order to avoid the computation of the inverse hysteresis model and nonlinear optimization problem, an inversion-free predictive controller,[29] and an adaptive Takagi-Sugeno fuzzy model-based predictive controller[30] are proposed. It is notable that MPC is practical and less complicated when it is designed according to the linear dynamic part of PEAs. It is reported that MPC has been successfully applied to achieve faster imaging in AFMs.[24,31] But the hysteresis is not considered in their applications.

The effect of hysteresis on the tracking performance of PEAs will be more evident with the increasing of the amplitude and frequency of the input signal. The hysteresis must be considered when large stroke and high frequency is required. A rate dependent LSSVM model is directly used for hysteresis identification and compensation.[32] In Ref. 32, the piezoactuated system is formed as a second-order linear system plus the hysteresis. The proposed approach based on the feedforward compensation is computational effective and has great potential for application in smart actuators. Micky Rakotondrabe develops a new feedforward hysteresis compensation method based on the inverse multiplicative structure.[33] He also extends the method to a two-degrees-of-freedom (2-dof) piezoactuator with the P-I hysteresis model.[34] The results show that the hysteresis has been completely removed through this method under low frequency range. The compensator is obtained as soon as the direct model is identified without complicated inversion.

In the literature, classical feedback controls have been employed, such as PID control, high-gain feedback control, state feedback control, etc., owing to their easy implementation.[35] In Ref. 36, an internal model-based feedback control combining feedforward compensation is designed. The internal model control is based on the inverse linear model and a low order filter. Compared with these methods, the MPC scheme is capable to achieve highly efficient control and operate for long periods of time. When the plant's model is well described, the MPC based method has good control performance, not compromised with higher order model and non-minimum phase system. Inspired by the inverse multiplicative structure, we propose a composite controller that a linear model predictive control with hysteresis compensation based on the inverse multiplicative structure. The feedforward compensator based on inverse multiplicative structure is effective and simple. The MPC plays as feedback control.

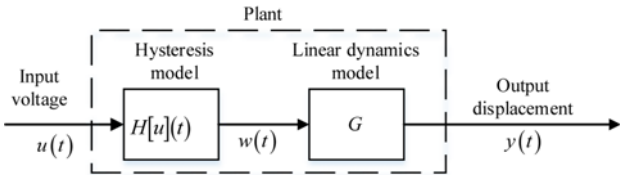

Fig. 1 The cascaded model of the piezo-actuated stage

The nonlinear dynamic behavior of a piezo-actuated stage is usually described by cascading hysteresis nonlinearity submodel with linear dynamics submodel. First, the inverse multiplicative structure based on the hysteresis nonlinearity submodel is used as the feedforward compensator. The classical Prandtl-Ishlinskii (P-I) model is an effective method to describe the hysteresis nonlinearity.[34] This paper adopts the classical P-I model for constructing the feedforward compensator. Then the MPC is designed according to the linear dynamics submodel, where it plays like a variable gain proportional controller. As a result, an integral type error compensation term is added to enhance the tracking performance, especially when the PEA's model is not well described. Experiments are conducted on a commercial nanopositioner to verify the effectiveness of the proposed composite controller. Furthermore, the proposed method is compared with the feedforward hysteresis compensation method[30] and MPC[24] alone. The main contribution of this work is the development of a composite control algorithm for precision motion tracking of piezo-actuated nanopositioning stage in large stroke applications.

The remainder of this paper is organized as follows. Section 2 is a brief description of the system and identification approach. The composite controller design progress is presented in Section 3. Section 4 discusses the verification of the proposed controller. Finally, the paper is concluded in Section 5.

2. System Description and Identification

The piezo-actuated stage is modeled by cascading the nonlinear hysteresis and the dynamics, namely the Hammerstein-like model structure[11,30] as shown in Fig. 1, where $H[u](t)$ denotes the hysteresis nonlinearity, G represents the linear dynamics. In this paper, $H[u](t)$ is described by a rate-independent P-I hysteresis model.

2.1 P-I Hysteresis model

The classical P-I model is a class of hysteresis models in which the model is a superposition of several elementary operators. The one-side play operator[37] is adopted in this study due to the positive displacement

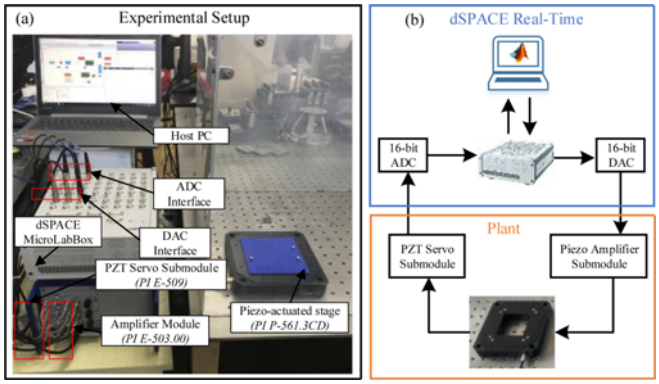

Fig. 2 The experimental setup of the piezo-actuated stage; (a) Experimental platform, (b) Block diagram of the signal flow

nature of the piezo-actuated stage. The operator $F_r[u](t)$ is defined by the following equations:

$$\begin{cases} F_r[u](0) = f_r(u(0),0) \\ F_r[u](t) = f_r(u(t), w(t-ts)) \end{cases} \quad (1)$$

$$f_r(u,w) = \max(u-r, \min(u,w)) \quad (2)$$

where, r is the threshold and ts is the refresh time.

The hysteresis model output $w(t)$ can be obtained by several operators each one having a threshold r_i and being weighted by q_i:

$$\begin{aligned} w(t) &= H[u](t) \\ &= \sum_{i=1}^{n} q_i \cdot F_{r_i}[u](t) = \sum_{i=1}^{n} q_i \cdot \max(u-r_i, \min(u,w)) \end{aligned} \quad (3)$$

where, n is the number of operators.

The parameters to be identified are the thresholds r_i and weight coefficients q_i.

2.2 Experimental setup

The experimental setup is developed and shown in Fig. 2. According to Fig. 2, the setup is composed of a three-axis nanopositioner (P-561.3CD), a dSPACE MicrolabBox, a piezo amplifier module (E-503.00, Physik Instrumente) with a fixed gain of 10, a sensor monitor (E-509.C3A, Physik Instrumente) and the host PC. The control input voltage range is (0-10 V). And the output voltage range is (0-10 V), which is normalized with respect to 0-100 μm. Details about the signal flow refer to Fig. 5(b). The control algorithm is designed in Matlab/ Simulink block diagram on the host PC, and then downloaded and executed on the target dSPACE MicroLabBox in the real-time software environment of dSPACE ControlDesk. When conducting experiments, only the x axis is adopted to implement the proposed controller and the sample rate is set to 5 kHz.

2.3 Identification approach

2.3.1 the dynamics model identification

From the previous discussion, there are two parts to be identified using the input and output data from the stage respectively. It is well known in the literature that the effect of hysteresis can be ignored in the displacement response if small-amplitude input excitation signals are applied. In the first step, to obtain the dynamic model, a small amplitude sine-sweep input voltage is able to identify the transfer function of the linear dynamics submodel. The model can be identified by the system identification toolbox in matlab.

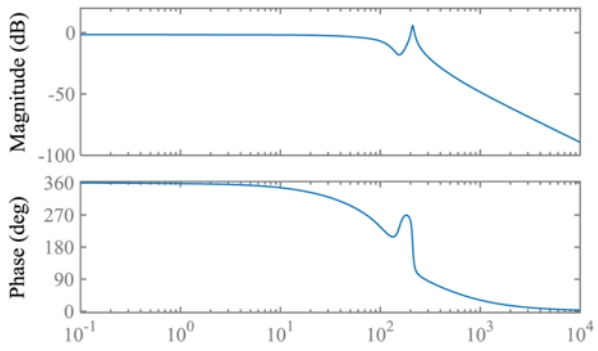

Fig. 3 bode plot of the identified linear dynamics model

The linear dynamics model is identified by applying a sine-sweep input voltage with a constant amplitude of 200 mv between 0.1 Hz and 500 Hz to the x axis. Notice that the low amplitude of the input voltage is used to excite the system for avoiding the effect of hysteresis nonlinearity. In this case, the hysteresis $H[u](t)$ is approximated as a constant 1. the input voltage and the output displacement data taken from the sensor are imported to matlab system identification toolbox to identify the model. The identified frequency response is shown in the Fig. 3.

The discrete dynamic model can be written in a state-space form,

$$\begin{cases} x(k+1) = A_d x(k) + B_d u(k) \\ y(k) = C_d x(k) + D_d u(k) \end{cases} \quad (4)$$

With,

$$A_d = \begin{bmatrix} 3.236 & -2.627 & 1.401 & -0.979 & 0.4128 & -0.321 \\ 2 & 0 & 0 & 0 & 0 & 0 \\ 0 & 2 & 0 & 0 & 0 & 0 \\ 0 & 0 & 1 & 0 & 0 & 0 \\ 0 & 0 & 0 & 1 & 0 & 0 \\ 0 & 0 & 0 & 0 & 0.25 & 0 \end{bmatrix}$$

$$B_d = [0.5 \quad 0 \quad 0 \quad 0 \quad 0 \quad 0]^T$$

$$C_d = [0.001362 \quad 0.1425 \quad -0.113 \quad 0.06919 \quad -0.002594 \quad -0.09873]$$

$$D_d = [0]$$

2.3.2 the hysteresis model identification

With the identified linear dynamics model, it is ready to identify the parameters of the classical P-I hysteresis model. In this step, the input signal is restricted in low frequency. Thus, the identified linear dynamics model can be directly recognized as a constant gain.

The frequency of the input signal is restricted as 0.1 Hz. Under this situation, the linear dynamics is a constant $G(0.2j\pi) = 0.84$ as shown in Fig. 3. A sine input voltage is applied to the system. The amplitude of the sine signal is set as 5 V, corresponding to 50% of the maximum

Table 1 The identified parameters of the P-I hysteresis model

Number	1	2	3	4	5
r_i	0	0.5	1.0	1.5	2.0
q_i	0.8353	0.1803	0.0636	0.0821	0.0665
Number	6	7	8	9	10
r_i	2.5	3.0	3.5	4.0	4.5
q_i	0.0653	0.0534	0.0756	-0.0170	0.2653

allowable input. Using the sine signal $u(t) = 5\sin(0.2\pi t)$ fed to the system, the output displacement $y(t)$ is recorded and pretreated before identification. We plot the output $y(t)$ versus to the input $u(t)$. The pretreatment includes intercepting the steady state part and removing the bias constant.

The number of operator n needs to be chosen reasonably. Generally, the model is more accurate with the increasing of n. However, a high number means increaseing its complexity. There is a compromise between accuracy and complexity. In our case, the number n is set as 10. The thresholds r_i are given by uniform partitions in the voltage domain.

$$r_i = \frac{i-1}{n}\|u(t)\|_\infty, i = 1,2,\cdots n \tag{5}$$

Due to the input signal is $u(t) = 5\sin(0.2\pi t)$, the thresholds is obtained. Then, weight coefficients q_i is to be determined through identification algorithms. Many algorithms have been developed for the identification of the hysteresis models. In this study, the least square method is adopted as an illustration. Table 1 lists the identified parameters of the P-I hysteresis model.

In order to evaluate the above identified model, Figs. 4 and 5 show the comparisons of the experimental data of the plant and the predictive results of the P-I model. In Fig. 4, the input voltage is a sine wave with variable amplitude. Fig. 4(c) shows that the maximal prediction error is about 0.92% and the root mean square (RMS) error is about 0.42% as a percentage of the full displacement range. The input voltage is a complex signal in Fig. 5. The maximal prediction error is about 1.8% and the root mean error is about 0.78%. According to the results shown in Figs. 4 and 5, the root mean errors between the experiment date the P-1 model are all less than 1%. These results demonstrate that the identified model is effective in characterizing the hysteresis.

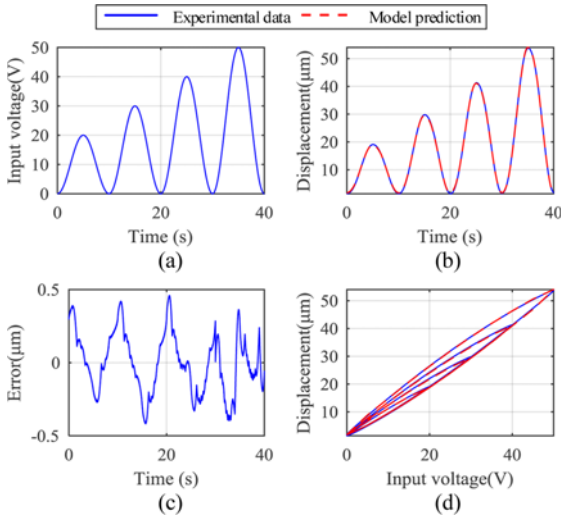

Fig. 4 Experimental verification of the identified P-I hysteresis model with a sine wave of variable amplitude; (a) Input voltage, (b) Displacement, (c) Error, (d) Hysteresis loop

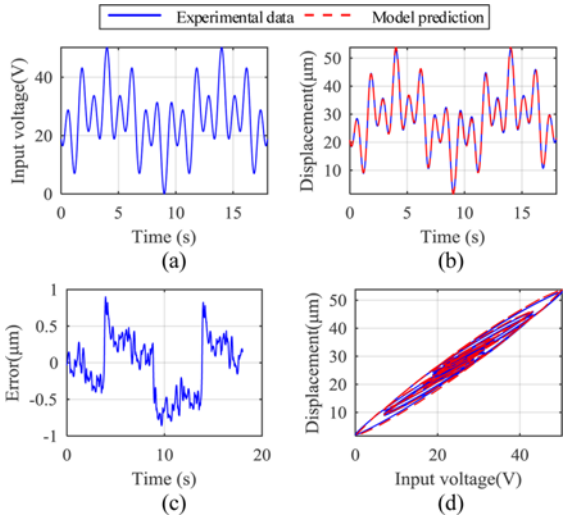

Fig. 5 Experimental verification of the identified P-I hysteresis model with a complex signal; (a) Input voltage, (b) Displacement, (c) Error, (d) Hysteresis loop

3. Design of the Composite Controller

The proposed controller in this paper is shown in Fig. 6, including feedforward hysteresis compensator based on the inverse multiplicative structure and the linear MPC. $y_r(t)$ is the desired reference trajectory, $v(t)$ is the control signal, $u(t)$ is the manipulated variable, and $y(t)$ is the output displacement.

3.1 Inverse multiplicative structure for hysteresis compensation

Considering the feedforward hysteresis compensator in Fig. 6, it is presented in Fig. 7 for analysis.

The control law is written by:

$$u(t) = v(t) + u(t-ts) - H[u](t-ts) \tag{6}$$

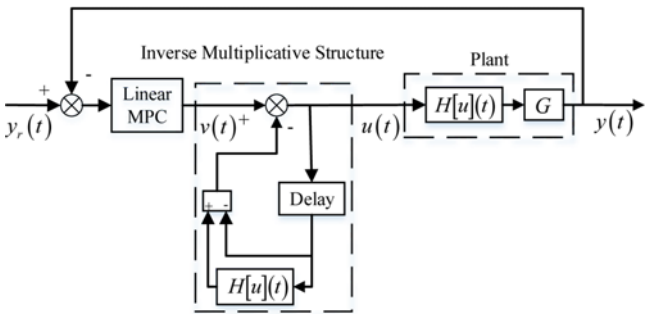

Fig. 6 Block diagram of the composite control structure

where, $H[u](t)$ is defied by Eq. (3).

Rewrite the model in Eq. (3),

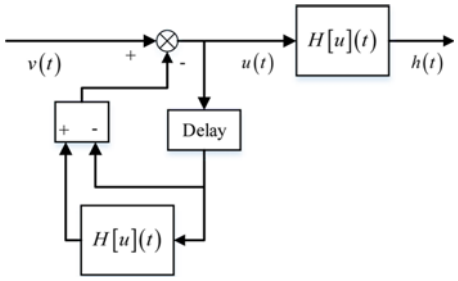

Fig. 7 Block diagram of the feedforward controller based on the inverse multiplicative structure

$$h(t) = H[u](t) = -u(t) + u(t) + H[u](t) \tag{7}$$

Assume the relationship between the actual output $h(t)$ and the control signal $v(t)$ is:

$$h(t) = v(t) + O(t) \tag{8}$$

Union Eqs. (6) and (7), the expression of O is obtained,

$$O = u(t-ts) - u(t) + H[u](t) - H[u](t-ts) \tag{9}$$

Calculate the derivative of the output $h(t)$ with respect to the control signal $v(t)$ by Eq. (8):

$$\begin{aligned} \frac{d(h(t))}{d(v(t))} &= \frac{d(v(t))}{d(v(t))} + \frac{d(O(t))}{d(v(t))} \\ &= \frac{\partial v(t)}{\partial v(t)} + \frac{\partial O(t)}{\partial v(t)} = 1 + \frac{\partial O(t)}{\partial v(t)} \end{aligned} \tag{10}$$

From Eq. (9), we have:

$$\begin{aligned} \frac{d(O(t))}{d(v(t))} &= \frac{d(u(t-ts)-u(t))}{d(v(t))} + \frac{d(H[u](t)-H[u](t-ts))}{d(v(t))} \\ &= \left[\frac{\partial u(t-ts)}{\partial v(t)} - \frac{\partial u(t)}{\partial v(t)}\right] + \left[\frac{\partial H[u](t)}{\partial v(t)} - \frac{\partial H[u](t-ts)}{\partial v(t)}\right] \end{aligned} \tag{11}$$

On the one hand, since the model $H[u](t)$ is independent of the control signal $v(t)$, it is inevitable:

$$\frac{\partial H[u](t)}{\partial v(t)} - \frac{\partial H[u](t-ts)}{\partial v(t)} = 0 \tag{12}$$

For a sampling time with ts, that is small enough relative to the period of the control signal $v(t)$, we have,

$$\left|\frac{\partial u(t-ts)}{\partial v(t)} - \frac{\partial u(t)}{\partial v(t)}\right| \to 0 \tag{13}$$

The detailed proof is presented in Ref. 34.

Combing Eqs. (11), (12) and (13), we get that,

$$d(O) \approx 0 \tag{14}$$

Substitute Eq. (14) into Eq. (10),

$$\frac{d(h(t))}{d(v(t))} = 1 + \frac{\partial O(t)}{\partial v(t)} \quad 1 \tag{15}$$

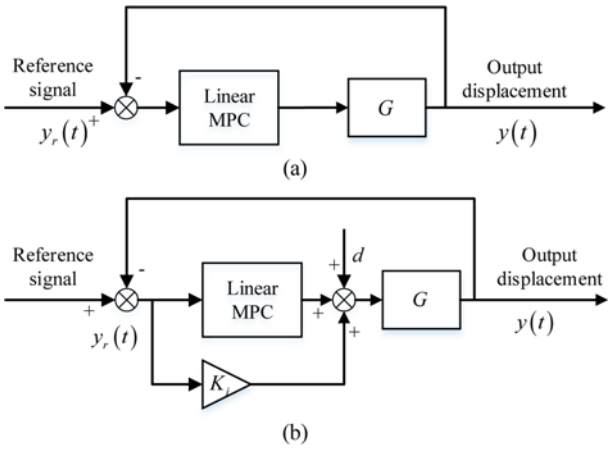

Fig. 8 (a) The equivalent diagram. (b) The equivalent diagram with integral error compensation

Eq. (15) implies:

$$h(t) \approx v(t) \tag{16}$$

Thus, it can be concluded that the hysteresis $H[u](t)$ is nearly compensated through this method.

It should be mentioned that when it comes to the practical application, the hysteresis model is required to be accurate respect to the actual hysteresis of PEAs for great compensation performance.

3.2 MPC with error compensation

Notice that the feedforward compensator is effective for removing the hysteresis nonlinearity. So The proposed control scheme in Fig. 2 can be reasonably reduced to the equivalent diagram in Fig. 8(a) for the design of MPC. The main goal of MPC is to enable the plant to track the reference signal. In MPC, a class of computer control algorithms use the identified process model to predict the future behavior of a plant. The control action is generated by minimizing the difference between the desired output and the predictive output.

3.2.1 Design of MPC

The linear dynamics model can be written as the discrete state-space model in the form,

$$\begin{cases} x(k+1) = A_d x(k) + B_d u(k) \\ y(k) = C_d x(k) \end{cases} \tag{17}$$

where, Ad, B_d, C_d define the discrete state-space model, u is the manipulated variable, y is the predictive output.

Making,

$$\begin{cases} \Delta x(k+1) = x(k+1) - x(k) \\ \Delta y(k+1) = y(k+1) - y(k) \\ \Delta u(k+1) = u(k+1) - u(k) \end{cases} \tag{18}$$

Eq. (17) can be rewritten as

$$\begin{cases} \Delta x(k+1) = A_d \Delta x(k) + B_d \Delta u(k) \\ y(k+1) = C_d A_d \Delta x(k) + y(k) + C_d B_d \Delta u(k) \end{cases} \tag{19}$$

Letting $x(k) = [\Delta x(k)\ y(k)]^T$, Eq. (19) is simplified as,

$$\begin{cases} x(k+1) = Ax(k) + B\Delta u(k) \\ y(k) = Cx(k) \end{cases} \tag{20}$$

where, A, B, $C$are the augmented system matrices.

$$A = \begin{bmatrix} A_d & 0 \\ C_d A_d & I \end{bmatrix},\ B = \begin{bmatrix} B_d \\ C_d B_d \end{bmatrix},\ C = [0\ I]$$

The predictive output sequence in the matrix form are then derived as,

$$Y = Fx(k) + \Phi\Delta U \tag{21}$$

in which,

$$Y = \begin{bmatrix} y(k+1|k) \\ y(k+2|k) \\ \vdots \\ y(k+N_p|k) \end{bmatrix},\ \Delta U = \begin{bmatrix} \Delta u(k) \\ \Delta u(k+1) \\ \vdots \\ \Delta u(k+N_c-1) \end{bmatrix}$$

N_p, N_c are the prediction horizon and the control horizon respectively.

The F matrix with the dimensions of (N_p, n) and the Φ matrix with the dimensions of (N_p, N_c) are:

$$F = \begin{bmatrix} CA \\ CA^2 \\ \vdots \\ CA^{N_p} \end{bmatrix},\ \Phi = \begin{bmatrix} CB & 0 & \cdots & 0 \\ CAB & CB & \cdots & 0 \\ \vdots & \vdots & \ddots & \vdots \\ CA^{N_p-1}B & CA^{N_p-2}B & \cdots & CA^{N_p-N_c}B \end{bmatrix}$$

The cost function is defied by,

$$J = \left[Y - R_s\right]^T Q\left[Y - R_s\right] + \Delta U^T R\Delta U \tag{22}$$

in which, Q and R are the adjustable weight matrices.

$$Q = \begin{bmatrix} Q_0 & & & \\ & Q_0 & & \\ & & \ddots & \\ & & & Q_0 \end{bmatrix},\ R = \begin{bmatrix} R_0 & & & \\ & R_0 & & \\ & & \ddots & \\ & & & R_0 \end{bmatrix}.$$

R_s is the reference signal,

$$R_s = \begin{bmatrix} r(k+1|k) \\ r(k+2|k) \\ \vdots \\ r(k+N_p|k) \end{bmatrix}$$

The control law is obtained by minimizing the value of the cost function J.

If the constraints of the manipulated variable are not considered, the control law can be obtained by taking the derivative of the cost function and setting it to zero, i.e.,

$$\frac{\partial J}{\partial \Delta U} = 0 \tag{23}$$

This results in,

$$\Delta U = \left(\Phi^T Q\Phi + R\right)^{-1}\Phi^T Q\left(R_s(k) - Fx(k)\right) \tag{24}$$

By considering the constraints, the control law is solved by minimizing J, subject to the linear inequality constraints on the manipulated variable, i.e.,

$$\begin{cases} u_{\min} \le u(k+i-1) \le u_{\max}, i = 1,\cdots,N_c \\ \Delta u_{\min} \le \Delta u(k+i-1) \le \Delta u_{\max}, i = 1,\cdots,N_c \end{cases} \tag{25}$$

u_{min} and u_{max} are the lower and upper bounds on the manipulated variable respectively, Δu_{min} and Δu_{max} lower and upper bounds on the control increments respectively.

The constrained MPC problem can be expressed as a quadratic programming (QP) problem, similar to that in Ref. 29.

3.2.2 MPC with integral error compensation

The first entry of ΔU in Eq. (24) is used for the controller design,

$$\Delta u(k) = \Psi R_s - \Psi F_2 y(k) - \Psi F_1 \Delta x(k) \tag{26}$$

Herein, the real control law can be written as follows:

$$\begin{aligned} & u(k) = u(k-1) + \Delta u(k) \\ & \Rightarrow \left(1 - z^{-1}\right)u(k) = \Psi R_s - \Psi F_2 y(k) - \Psi F_1 \Delta x(k) \\ & \Rightarrow u(k) = \Psi_1 R_s - \Psi_1 F_2 y(k) - \Psi_1 F_1 \Delta x(k) \end{aligned} \tag{27}$$

where, Ψ is the first row of $(\Phi^T Q\Phi+R)^{-1}\Phi^T Q$, F = [$F_1$ F_2], and $\Psi_1 = \Psi/(1-z^{-1})$.

It can be seen that the control law is similar to a proportional control. When the PEA's model is not well described, the steady-state error is obvious. An integral type error compensation term is useful for reducing the steady-state error.

The error compensation term is defined as,

$$\Delta u_e(k) = K_i\left(r(k) - y(k)\right) \tag{28}$$

in which, K_i is the gain of the integral term.

The final control law is obtained by using the error compensation term to modify,

$$u(k) = \Psi_1 R_s - \Psi_1 F_2 y(k) - \Psi_1 F_1 \Delta x(k) + \Delta u_e(k) \tag{29}$$

The block diagram of the control loop based on Eq. (22) is illustrated in Fig. 8(b). d is the input disturbance.

4. Experimental Results

4.1 Verification of MPC with integral error compensation

The linear MPC is effective in tracking the reference spiral line in Ref. 31 without considering the hysteresis. It is reasonable not to consider the hysteresis phenomenon with the small scanning range. When the application is extended to large stroke, the effect of hysteresis nonlinearity is obvious. The linear dynamics model can't approximate the behavior of the plant well. In this case, the steady-state error is relatively large with only using the linear MPC.[27] The integral error compensation is useful to reducing the steady-state error. The corresponding parameters are set as N_p = 4, N_c = 3, K_i = 595, Q_0 = 1, R_0 = 0.1. Fig. 9 shows the comparison.

4.2 Verification of the proposed controller

The experiments are conducted to verify the effectiveness of the

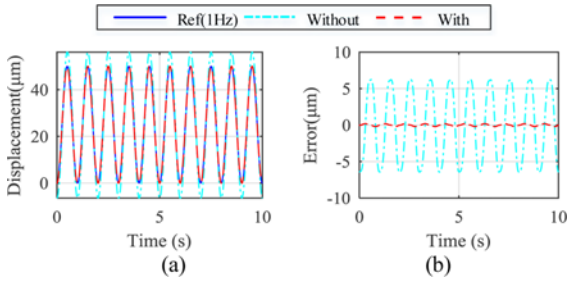

Fig. 9 Comparison between linear MPC with integral error compensation and without; (a) Reference and actual position trajectories, (b) Tracking errors

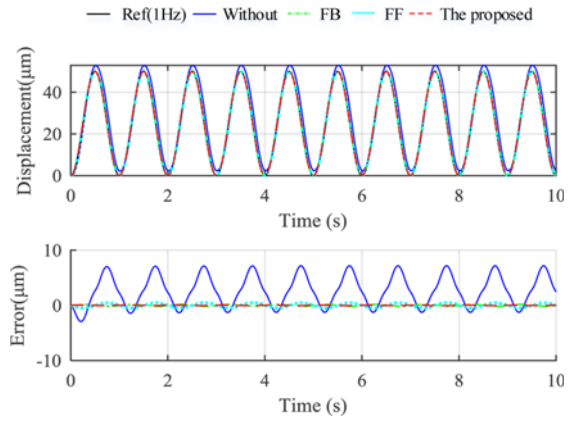

Fig. 10 Experimental results with 1 Hz sine references; (a) Reference and actual position trajectories, (b) Tracking errors

proposed controller. Sinusoidal waves with different frequency and complex signals are applied in the tracking experiments. The prediction and control horizon parameters N_p and N_c ($N_p \geq N_c$) are determined through simulation. Under the premise of ensuring tracking accuracy, we choose $N_p = 4$, $N_c = 3$ for reducing the computational burden. The other parameters are set as $K_i = 350$, $Q_0 = 1$, $R_0 = 0.1$ by trial and error. And the proposed method is compared with the feedforward hysteresis compensation method and the linear MPC. For a quantitative analysis, the root-mean-square error (RMSE) and maximum absolute error (MAXE) are defined as follows:

$$e_{\mathrm{RMS}} = \sqrt{\left(\sum_{i=1}^{N} e_i^2\right)/N} \tag{30}$$

$$e_{\mathrm{MAX}} = \max\left(|e|\right) \tag{31}$$

where, N is the number of data sets.

First, the motion tracking of a 1 Hz sinusoidal trajectory is tested, as shown in Fig. 10. The RMSE and MAXE of 3.878 and 7.173 μm exist in open loop without controller, which are equivalent to 7.329% and 13.558% of the motion range. And the proposed controller achieves best performance with the RMSE and MAXE of 0.043 and 0.085 μm, equivalent to 0.087% and 0.169% of the motion range. As a result, the positioning accuracy with the proposed controller has been improved by 98.8% compared with open loop without controller.

It is observed that the feedforward hysteresis compensation method

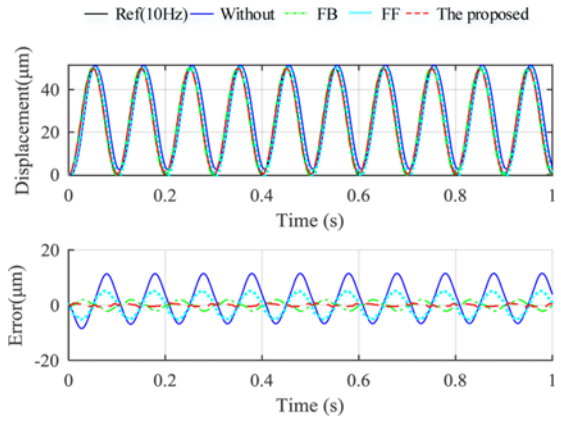

Fig. 11 Experimental results with 10 Hz sine references; (a) Reference and actual position trajectories, (b) Tracking errors

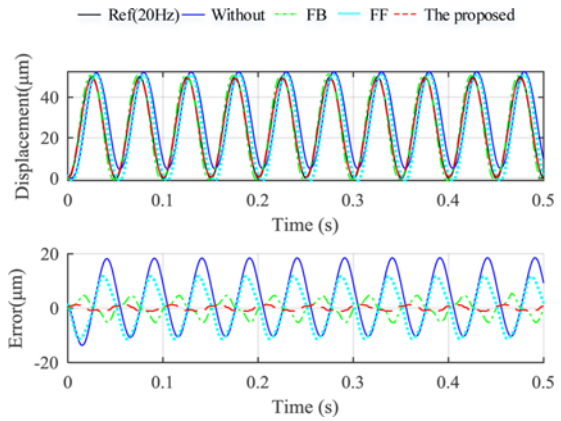

Fig. 12 Experimental results with 20 Hz sine references; (a) Reference and actual position trajectories, (b) Tracking errors

produces RMSE and MAXE of 0.346 and 0.500 μm. The linear MPC alone produces RMSE and MAXE of 0.123 and 0.198 μm. As compared with the feedforward hysteresis compensation method, the linear MPC reduces RMSE and MAXE by 64% and 60%, and the proposed method reduces RMSE and MAXE by 87% and 83% respectively.

Moreover, the tracking results of references with different frequency 10 Hz, 20 Hz and 50 μm amplitude are generated, shown in Figs. 11 and 12 respectively.

Next, the motion tracking of complex signals *CS*, with $f_{max} = 0.9$ Hz and $f_{max} = 9$ Hz is examined, as shown in Figs. 13 and 14 respectively. The complex signal *CS* contains different amplitude and frequency components. Similarly, the proposed method achieves best performance.

$$CS = 0.77\left(1-\cos\left(\frac{2\pi f_{\max}}{9}t\right)\right) + 0.69\left(1-\cos\left(\frac{10\pi f_{\max}}{9}t\right)\right) + 1.05\left(1-\cos\left(2\pi f_{\max}t\right)\right) \tag{32}$$

For a clear presentation, Tables 2 and 3 list the value of RMSE and MAXE tracking errors of the three controllers and the corresponding percentage versus the total stroke. It can be learned that the proposed controller performs better than the feedforward hysteresis compensation method and the linear MPC in terms of motion tracking accuracy.

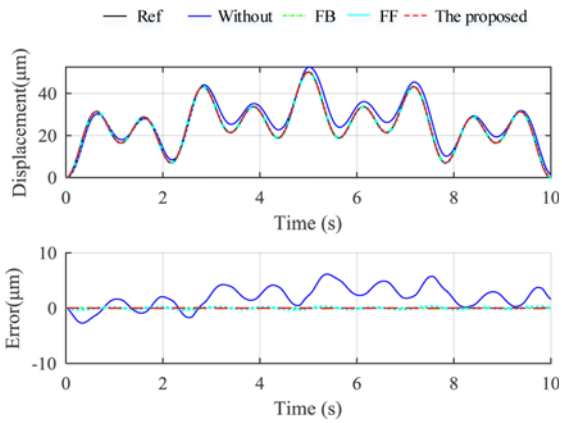

Fig. 13 Experimental results with f_{max} = 0.9 Hz complex signals; (a) Reference and actual position trajectories, (b) Tracking errors

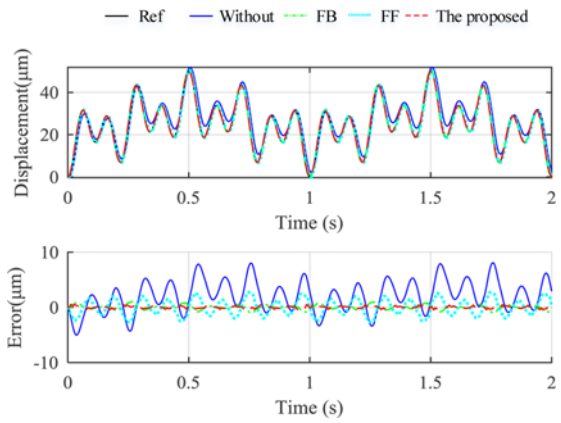

Fig. 14 Experimental results with f_{max} = 9 Hz complex signals; (a) Reference and actual position trajectories, (b) Tracking errors

Table 2 The value of RMSE and percentage versus the total stroke

Input signal	Frequency (Hz)	Without (μm / %)	FF (μm / %)	MPC (μm / %)	The proposed (μm / %)
Sine	1	3.878 / 7.329	0.346 / 0.692	0.123 / 0.245	0.043 / 0.087
	10	6.588 / 12.78	3.629 / 7.137	1.269 / 2.518	0.407 / 0.819
	20	10.76 / 20.47	7.846 / 15.03	2.899 / 5.540	0.837 / 1.727
CS	f_{max} = 0.9	2.839 / 5.404	0.136 / 0.270	0.038 / 0.075	0.021 / 0.042
	f_{max} = 9	3.512/ 6.773	1.421 / 2.789	0.380 / 0.754	0.210 / 0.416

Table 3 The value of MAXE and percentage versus the total stroke

Input signal	Frequency (Hz)	Without (μm / %)	FF (μm / %)	MPC (μm / %)	The proposed (μm / %)
Sine	1	7.173 / 13.558	0.500 / 0.999	0.199 / 0.397	0.085 / 0.169
	10	11.52 / 22.35	5.151 / 10.129	1.992 / 3.952	0.751 / 1.511
	20	18.55 / 35.31	11.723 / 22.46	5.423 / 10.363	1.343 / 2.771
CS	f_{max} = 0.9	6.147 / 11.69	0.279 / 0.554	0.102 / 0.203	0.059 / 0.118
	f_{max} = 9	8.063 / 15.55	2.715 / 5.329	1.053 / 2.088	0.526 / 1.044

5. Conclusions

In this paper, a composite controller is proposed for precision tracking of a piezo-actuated stage. It consists of a linear MPC with integral error compensation and a feedforward static hysteresis compensation based on inverse multiplicative structure. The main advantages lie in avoiding the inverse of hysteresis model and the simple solution of the linear MPC. After setting of the prediction horizon and the control horizon of MPC, there are only three parameters to turn. The implement of the proposed control is convenient in practical applications. The tracking experiments are conducted on the constructed test platform. The results verify its effectiveness.

In this work, the steady-state error is reduced by an integral error compensation term. However, the control with constraints can be hardly dealt with. We will try to incorporate the integral term in the MPC algorithm in the future work.

ACKNOWLEDGEMENT

This work was supported by *Shenzhen Science and Technology Program* (grant JCYJ20170306171514468).

REFERENCES

1. Kenton, B. J. and Leang, K. K., "Design and Control of a Three-Axis Serial-Kinematic High-Bandwidth Nanopositioner," IEEE/ASME Transactions on Mechatronics, Vol. 17, No. 2, pp. 356-369, 2012.
2. Feng, Z., Ling, J., Ming, M., and Xiao, X.-H., "High-Bandwidth and Flexible Tracking Control for Precision Motion with Application to a Piezo Nanopositioner," Review of Scientific Instruments, Vol. 88, No. 8, Paper No. 085107, 2017.
3. Salapaka, S. M. and Salapaka, M. V., "Scanning Probe Microscopy," IEEE Control Systems, Vol. 28, No. 2, pp. 65-83, 2008.
4. Mahmood, I. A. and Moheimani, S O. R., "Making a Commercial Atomic Force Microscope More Accurate and Faster Using Positive Position Feedback Control," Review of Scientific Instruments, Vol. 80, No. 6, Paper No. 063705, 2009.
5. Ling, J., Feng, Z., Ming, M., and Xiao, X., "Damping Controller Design for Nanopositioners: A Hybrid Reference Model Matching and Virtual Reference Feedback Tuning Approach," International Journal of Precision Engineering and Manufacturing, Vol. 19, No. 1, pp. 13-22, 2018.

6. Gu, G.-Y., Zhu, L.-M., Su, C.-Y., Ding, H., and Fatikow, S., "Modeling and Control of Piezo-Actuated Nanopositioning Stages: A Survey," IEEE Transactions of Automation Science and Engineering, Vol. 13, No. 1, pp. 313-332, 2016.

7. Ang, K. H., Chong, G., and Li, Y., "PID Control System Analysis, Design, and Technology," IEEE Transactions on Control Systems Technology, Vol. 13, No. 4, pp. 559-576, 2005.

8. Xiao, S., Li, Y., and Liu, J., "A Model Reference Adaptive PID Control for Electromagnetic Actuated Micro-Positioning Stage," Proc. of IEEE International Conference on Automation Science and Engineering (CASE), pp. 97-102, 2012.

9. Tang, H. and Li, Y., "Feedforward Nonlinear PID Control of a Novel Micromanipulator Using Preisach Hysteresis Compensator," Robotics and Computer-Integrated Manufacturing, Vol. 34, pp. 124-132, 2015.

10. Aridogan, U., Shan, Y., and Leang, K. K., "Design and Analysis of Discrete-Time Repetitive Control for Scanning Probe Microscopes," Journal of Dynamic Systems, Measurement, and Control, Vol. 131, No. 6, Paper No. 061103, 2009.

11. Ling, J., Feng, Z., Yao, D., and Xiao, X., "A Position Domain Iteration Learning Control for Contour Tracking with Application to a Multi-Axis Motion Testbed," Proc. of American Control Conference (ACC), pp. 1247-1252, 2016.

12. Feng, Z., Ling, J., Ming, M., and Xiao, X., "A Model-Data Integrated Iterative Learning Controller for Flexible Tracking with Application to a Piezo Nanopositioner," Transactions of the Institute of Measurement and Control, Vol. 40, No. 10, pp. 3201-3210, 2018.

13. Li, Y., and Xu, Q., "Design and Robust Repetitive Control of a New Parallel-Kinematic XY Piezostage for Micro/Nanomanipulation," IEEE/ASME Transactions on Mechatronics, Vol. 17, No. 6, pp. 1120-1132, 2012.

14. Liaw, H. C., Shirinzadeh, B., and Smith, J., "Enhanced Sliding Mode Motion Tracking Control of Piezoelectric Actuators," Sensors and Actuators A: Physical, Vol. 138, No. 1, pp. 194-202, 2007.

15. Mobayen, S. and Baleanu, D., "Stability Analysis and Controller Design for the Performance Improvement of Disturbed Nonlinear Systems Using Adaptive Global Sliding Mode Control Approach," Nonlinear Dynamics, Vol. 83, No. 3, pp. 1557-1565, 2016.

16. Xu, Q., "Digital Sliding-Mode Control of Piezoelectric Micropositioning System Based on Input-Output Model," IEEE Transactions of Industrial Electronics, Vol. 61, No. 10, pp. 5517-5526, 2014.

17. Xu, Q., "Precision Motion Control of Piezoelectric Nanopositioning Stage with Chattering-Free Adaptive Sliding Mode Control," IEEE Transactions on Automation Science and Engineering, Vol. 14, No. 1, pp. 238-248, 2017.

18. Peng, J. Y. and Chen, X. B., "Integrated PID-Based Sliding Mode State Estimation and Control for Piezoelectric Actuators," IEEE/ASME Trans. Mechatronics, Vol. 19, No. 1, pp. 88-99, 2014.

19. Xu, Q., "Continuous Integral Terminal Third-Order Sliding Mode Motion Control for Piezoelectric Nanopositioning System," IEEE/ASME Transactions on Mechatronics, Vol. 22, No. 4, pp. 1828-1838, 2017.

20. Tang, W. Q. and Cai, Y. L., "High-Order Sliding Mode Control Design Based on Adaptive Terminal Sliding Mode," International Journal of Robust and Nonlinear Control, Vol. 23, No. 2, pp. 149-166, 2013.

21. Wills, A. G., Bates, D., Fleming, A. J., Ninness, B., and Moheimani, S. R., "Model Predictive Control Applied to Constraint Handling in Active Noise and Vibration Control," IEEE Transactions on Control Systems Technology, Vol. 16, No. 1, pp. 3-12, 2008.

22. Qin, S. J. and Badgwell, T. A., "A Survey of Industrial Model Predictive Control Technology," Control Engineering Practice, Vol. 11, No. 7, pp. 733-764, 2003.

23. Vazquez, S., Leon, J. I., Franquelo, L. G., Rodriguez, J., Young, H. A., et al., "Model Predictive Control: A Review of Its Applications in Power Electronics," IEEE Industrial Electronics Magazine, Vol. 8, No. 1, pp. 16-31, 2014.

24. Rana, M. S., Pota, H. R., and Petersen, I. R., "Performance of Sinusoidal Scanning with MPC in AFM Imaging," IEEE/ASME Transactions on Mechatronics, Vol. 20, No. 1, pp. 73-83, 2015.

25. Xu, Q., "Digital Sliding Mode Prediction Control of Piezoelectric Micro/Nanopositioning System," IEEE Transactions on Control Systems Technology, Vol. 23, No. 1, pp. 297-304, 2015.

26. Xu, Q., "Digital Integral Terminal Sliding Mode Predictive Control of Piezoelectric-Driven Motion System," IEEE Transactions on Industrial Electronics, Vol. 63, No. 6, pp. 3976-3984, 2016.

27. Cao, Y., Cheng, L., Chen, X. B., and Peng, J., "An Inversion-Based Model Predictive Control with an Integral-of-Error State Variable for Piezoelectric Actuators," IEEE/ASME Transactions on Mechatronics, Vol. 18, No. 3, pp. 895-904, 2013.

28. Liu, W., Cheng, L., Hou, Z.-G., Yu, J., and Tan, M., "An Inversion-Free Predictive Controller for Piezoelectric Actuators Based on a Dynamic Linearized Neural Network Model," IEEE/ASME Transactions on Mechatronics, Vol. 21, No. 1, pp. 214-226, 2016.

29. Cheng, L., Liu, W., Hou, Z.-G., Yu, J., and Tan, M., "Neural-Network-Based Nonlinear Model Predictive Control for Piezoelectric Actuators," IEEE Transactions on Industrial Electronics, Vol. 62, No. 12, pp. 7717-7727, 2015.

30. Cheng, L., Liu, W., Hou, Z.-G., Huang, T., Yu, J., and Tan, M., "An Adaptive Takagi-Sugeno Fuzzy Model-Based Predictive Controller for Piezoelectric Actuators," IEEE Transactions on Industrial Electronics, Vol. 64, No. 4, pp. 3048-3058, 2017.

31. Rana, M. S., Pota, H. R., and Petersen, I. R., "Spiral Scanning with Improved Control for Faster Imaging of AFM," IEEE Transactions on Nanotechnology, Vol. 13, No. 3, pp. 541-550, 2014.

32. Xu, Q., "Identification and Compensation of Piezoelectric Hysteresis

without Modeling Hysteresis Inverse," IEEE Transactions on Industrial Electronics, Vol. 60, No. 9, pp. 3927-3937, 2013.

33. Rakotondrabe, M., "Bouc-Wen Modeling and Inverse Multiplicative Structure to Compensate Hysteresis Nonlinearity in Piezoelectric Actuators," IEEE Transactions on Automation Science and Engineering, Vol. 8, No. 2, pp. 428-431, 2011.
34. Rakotondrabe, M., "Multivariable Classical Prandtl-Ishlinskii Hysteresis Modeling and Compensation and Sensorless Control of a Nonlinear 2-DOF Piezoactuator," Nonlinear Dynamics, Vol. 89, No. 1, pp. 481-499, 2017.
35. Xu, Q. and Tan, K. K., "Advanced Control of Piezoelectric Micro-/Nano-Positioning Systems," Springer, 2016.
36. Al Janaideh, M., Rakotondrabe, M., Al-Darabsah, I., and Aljanaideh, O., "Internal Model-Based Feedback Control Design for Inversion-Free Feedforward Rate-Dependent Hysteresis Compensation of Piezoelectric Cantilever Actuator," Control Engineering Practice, Vol. 72, pp. 29-41, 2018.
37. Gu, G.-Y., Li, C.-X., Zhu, L.-M., and Su, C.-Y., "Modeling and Identification of Piezoelectric-Actuated Stages Cascading Hysteresis Nonlinearity with Linear Dynamics," IEEE/ASME Transactions on Mechatronics, Vol. 21, No. 3, pp. 1792-1797, 2016.

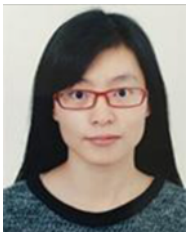

Min Ming
B.S degree in Mechanical Engineering from School of Power and Mechanical Engineering, Wuhan University, Wuhan, China, in 2016. She is currently pursuing the Ph.D. degree in Mechanical Engineering at Wuhan University, Wuhan, China. Her research interests include hysteresis control, model prediction control, nano-positioner.
E-mail: mingmin_whu@whu.edu.cn

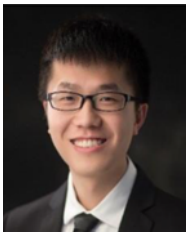

Jie Ling
B.S and Ph.D. degrees in Mechanical Engineering from School of Power and Mechanical Engineering, Wuhan University, Wuhan, China, in 2012 and 2018 respectively. He is currently a postdoctor in Mechanical Engineering at Wuhan University, Wuhan, China. His research interests include precise motion control, iterative learning control, nanopositioning and robotics.
E-mail: jamesling@whu.edu.cn

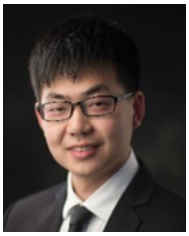

Zhao Feng
B.S degree in Mechanical Engineering from School of Power and Mechanical Engineering, Wuhan University, Wuhan, China, in 2014. He is currently pursuing the Ph.D. degree in Mechanical Engineering at Wuhan University, Wuhan, China. His research interests include vibration control, iterative learning control, nanopositioning and robotics.
E-mail: fengzhaozhao7@whu.edu.cn

Xiaohui Xiao
B.S. and M.S. degrees in Mechanical Engineering from Wuhan University, Wuhan, China, in 1991 and 1998, respectively, and the Ph.D. degree in mechanical engineering from Huazhong University of Science and Technology, Wuhan, China, in 2005. She joined the Wuhan University, Wuhan, China, in 1998, where she is currently a Full Professor with the Mechanical Engineering Department, School of Power and Mechanical Engineering. She has published over 30 papers in the areas of mobile robots, dynamics and control, sensors and signal procession. Her current research interests include mobile robotics, high-precision positioning control, and signal processing.
E-mail: xhxiao@whu.edu.cn